Fourth International Symposium on Marine Propulsors
SMP'15, Austin, Texas, USA, June 2015

Experimental Analysis of Strains and Vibratory Response of a Flexible Foil

Alexandra Lelong[1], Jacques-André Astolfi[2]

[1, 2] Department of Mechanical Engineering,
Naval Academy Research Institute, Lanvéoc-Poulmic, CC 600, 29240 BREST Cedex 9, France

ABSTRACT

The paper deals with an academic experimental study of the hydroelastic response of a flexible plastic hydrofoil undergoing various flow conditions including unsteady partial cavitating flow. It is based on the analysis of the vibrations, strains and stresses of a cantilevered hydrofoil made of POM, at Reynolds number ranging from 3. 10^5 to 6.10^5 in non cavitating flows. The vibration response was measured by means of two laser vibrometers in order to identify the modal response, mainly the first flexion and twisting modes. The strains and resulting stresses were obtained from integrated strain gauges imbedded in the foil close to the root section. A high speed camera was used in order to analyze unsteady features of the cavitating flow.

The paper presents the experimental setup and the main results are discussed. In fully wetted flow, it was shown that the twisting frequency increases with the flow velocity. In cavitating flow, the twisting mode's frequency increases as the cavitation develops on the foil surface suggesting the decrease of the added-mass in partially cavitating flow. The possibility of a lock-in of the flexion mode in interaction with the cavity oscillation, or its harmonics or sub-harmonics, was found for relatively large cavity. At the same time, the mean values of the strains and stresses of the foil tend to decrease, but their fluctuation intensities increase strongly as the number of cavitation decreases.

Keywords

flexible hydrofoil, cavitation, hydroelastic response, strains, vibration, fluid-structure interaction.

1 INTRODUCTION

The present work is developed within the general frame of new propeller designs using nonmetallic material. Several marine structures, like propellers or rudder, suffer from cavitation, which occurs when the pressure in the fluid is lower than its vapor pressure (Brennen (1995), Franc (2006)). It leads to material damages or noise, and induce high vibrations of the structures.

Moreover, these structures are subjected to high stresses due to the density of water, as shown by Søntvedt (1974) applying finite element method to determine the quasi-static and dynamic stresses in a propeller blade. These stresses can be quite different using nonmetallic and lighter materials such as composite or other soft materials. Gaugain et al (2012) realized a numerical and experimental study of a flexible hydrofoil in a steady flow. Numerical strains and stresses had then a pretty good agreement with experimental data.

For marine propellers using composite material to enhance hydrodynamics forces, to control the deformation of the structure and to control cavitation as well could be a promising way. However using light-flexible structures give rise to new questions about the hydro-elastic response of the structures in a heavy fluid undergoing high Reynolds and potentially two-phase cavitating flows. This includes several points that need to be well understood in such rather complex flows as added-mass effect due to heavy fluid in partially two-phase cavitating flow, damping effect and possible flow-structure instabilities as well. For example Benaouicha and Astolfi (2012) showed theoretically that partial cavitation changes the added-mass matrix on two-dimensional sections

Several numerical developments were developed to analyze fluid-structure interaction (FSI) of flexible composite marine propellers (Lin et al. (2005), Young (2007), Young (2008), Young et al (2009), Mulcahy et al (2010), Motley, & Young (2011)). However the numerical development suffers from a lack of experimental data. Indeed, a large number of experimental studies deals with the analysis of cavitation over rigid hydrofoils (Leroux et al (2005), Coutier-Delgosha et al (2007)) but little referred to experimental cavitation on flexible structures.

Recently, cavitation over a flexible hydrofoil has been studied experimentally by Ducoin et al (2009) and Ducoin et al (2012b), and numerically by Akcabay and Young (2014) and Akcabay et al. (2014). This study, as well as Benaouicha et al (2010), also deals with the vibration induced by the cavitation. Indeed, an important phenomenon of lock-in of the foil's frequencies in cavitating flows was shown by Reese (2010) and has to be taken in account to analyze the vibratory response of the structure.

The present paper deals with a collaborative research program with the Department of Naval Architecture and Marine Engineering at the University of Michigan in order to analyze the hydroelastic response of a flexible homogeneous hydrofoil in various flow conditions. The objective of the program is to perform physical analysis as well as to improve simulations for FSI applications.

2 EXPERIMENTAL SETUP

The experiments were carried out in the cavitation tunnel of Naval Academy Research Institute (IRENav). The test section is a 192mm square and is 1m long (Figure 1). The flow velocity can be chosen between 3 and 12m.s^{-1} and the pressure in the tunnel between 100mbar and 3bar to obtain cavitating flows. The turbulence intensity in the middle of the test section is close to 2%.

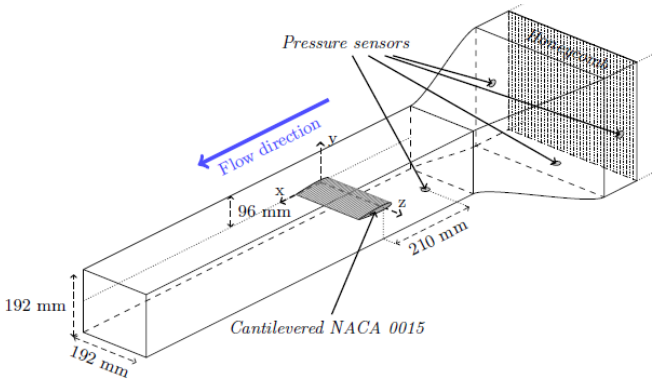

Figure 1: Cavitation tunnel of IRENav.

The foil is a flexible rectangular cantilevered NACA 0015, made in Polyoxymethylene plastic (POM). The chord length is c = 100mm and the span length is b = 191mm (Figure 2). The center of rotation of the foil is at mid chord. POM is an isotropic material, its characteristics are given in the Table 1 and compared with the steel's ones for information.

Figure 2: Flexible hydrofoil. Equipped with three identical strain gauges

The incidence of the foil in the tunnel is controlled by a Baldor® drive system that allows us to control with high accuracy the angle step $\Delta\alpha$, the acceleration and the rotational speed. The theoretical accuracy of the adjustment is 6.10^{-4} degree, however the uncertainties of the angle of attack was founded to be 0.1°, considering the mechanical mounting system.

	Steel	POM
Young mod. (E)	203 GPa	2.9 GPa
Poisson coef. (ν)	0.30	0.35
Density (ρ)	8010 kg.m^{-3}	1420 kg.m^{-3}

Table 1: Characteristics of the flexible material

2.1 Strain measurements

To determine independent components of plane strain, the hydrofoil is equipped with three identical strain gauges, which are glued in a hole close to the root of the foil (Figure 3a). The cavity is filled with a resin whose mechanical characteristics are close to the foil's material.

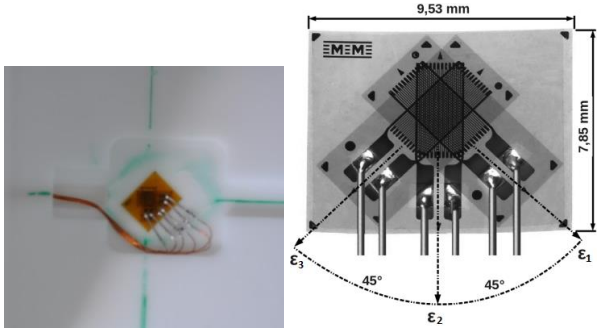

(a) (b)

Figure 3: Strain gauges fixed on the foil (a) and its diagram (b).

The strain gauges are L2A_13-125WW-120 from Vishay Micro Measurements. They are made in constantan and have a K-factor equal to 2.11. Their accuracy is ±6%. The strain gauges are assembled in a Quarter Bridge (Figure 3b). The strain gauges measure the strains $\varepsilon_{1,2,3}$ in the direction of their own axis. The gauges' axes are separated by a 45° angle and the first one is given by the span direction (ε_1), the third by the chord direction (ε_3). Their data are first amplified (Quantum mx16, HBM) and then recorded thanks to the acquisition software CATMAN (HBM).

The principal strains $\varepsilon_{I,II}$ can be calculated by:

$$\varepsilon_{I,II} = \frac{\varepsilon_1+\varepsilon_3}{2} \pm \frac{1}{2}\sqrt{(\varepsilon_3-\varepsilon_1)^2 + 4\cdot\left(\varepsilon_2 - \frac{1}{2}(\varepsilon_1+\varepsilon_3)\right)^2} \quad (1)$$

as well as the principal stresses $\sigma_{I,II}$:

$$\sigma_{I,II} = \lambda(\boldsymbol{\varepsilon}_I + \boldsymbol{\varepsilon}_{II}) + 2\mu\varepsilon_{I,II} \quad (2)$$

with $\lambda = {(E\nu)}/{(1+\nu)(1-2\nu)}$ and $\mu = {E}/{2(1+\nu)}$ the Lamé parameters.

The Von Mises stress can be computed as well by:

$$\sigma_{VM} = \sqrt{\sigma_I^2 + \sigma_{II}^2 - \sigma_I \cdot \sigma_{II}} \qquad (3)$$

2.2 Vibration measurements

The measurements were performed with two vibrometers from Polytec: the first one is fixed and is the reference; the second one is a PSV-400 scanning vibrometer. This model can detect vibrations up to 10m.s^{-1} with a HeNe laser (λ = 633nm). It is equipped with two analog velocity decoder VD-04 and VD-06. The scanner is a high precision scan unit, with an angular resolution lower than 0.002° and an angular stability lower than 0.01° per hour.

The measurement points are on the pressure side and close to the free tip of the foil (Figure 4). The reference is approximatively the middle cord (green point). Concerning the scanning vibrometer, two points were recorded on both sides of the reference point: one close to the leading edge, the second one close to the trailing edge (red points). Because of laser light diffusion in the POM material, reflecting adhesive tapes were glued on the foil's surface to enhance the signal noise ratio.

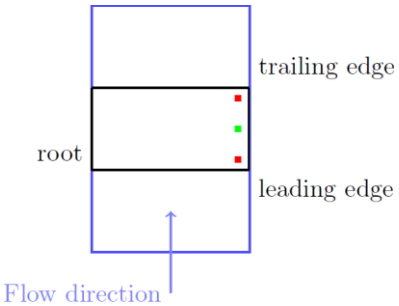

Figure 4: Vibration measurement points on the foil's surface (green: reference, red: scanning vibro.)

A high speed camera was fixed over the test section to record movies when cavitation develops over the foil. The model used is a Fastcam SA3 120K from Photron. It is equipped with a CMOS image sensor, which sensor size is 17.4mm*17.4mm. The frame rate is spread from 60fps to 2000fps for the full sensor resolution (1024*1024 pixels), when the pixel size is 17µm. The global experimental configuration is shown on Figure 5.

An electrodynamic shaker was also used to measure the response of the foil to an impulse and identify the natural frequencies of the foil in air and in still water. Eight measurements were performed in each case, with one impulse per measurement, and the mean spectrum was calculated.

The modes have been identified thanks to the phase difference between the reference and the measurement points of the scanning vibrometer. The spectra are shown on Figure 6 and the values of the three first modes' frequencies are given in the Table 2. The frequency resolution of the following measurements is Δf = 0.625Hz. The repeatability

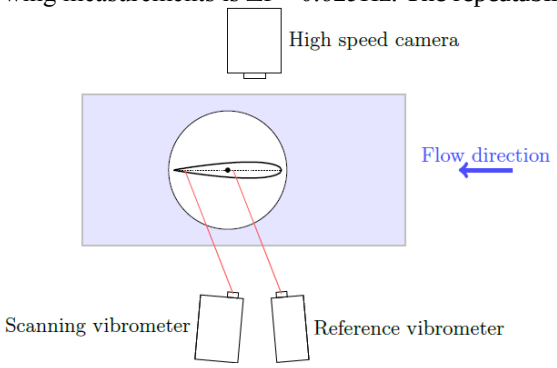

Figure 5: Test section in experimental configuration.

of the experiment was tested and the accuracy was then lower than 2%. As shown, the frequencies of the bending (f_1) and twisting (f_2) modes in water decrease strongly compared to in the air as a result of added mass effects.

	Air	Still water
f_1	80.6	34.4
f_2	390	183.5
f_3	556.5	292

Table 2: First modes' frequencies as response to series of eight impulses (Hz)

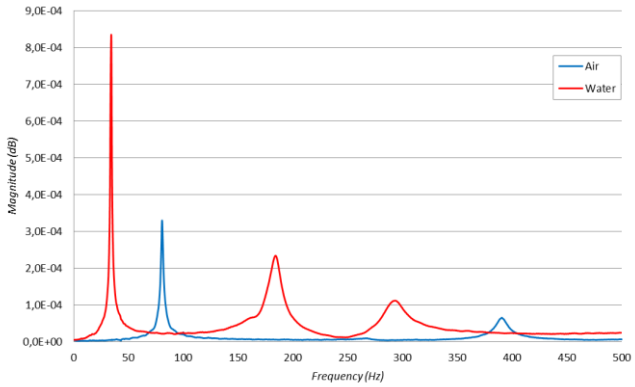

Figure 6: Response of the foil to an impulse in m.s^{-1}.

3 FOIL'S VIBRATION

3.1 Non cavitating flow

Measurements were carried out at a constant pressure in the tunnel section close to the atmospheric pressure, for which cavitation does not develop. They were performed for angles of incidence from 0° to 8° with a step Δα = 2°, the flow velocity was 3, 4, 5 and 6 m.s^{-1}, corresponding to Reynolds numbers based on the chord length ranging from 3.10^5 to 6.10^5. The frequencies of the first two modes, which correspond to bending and twisting modes, are reported on Table 3 for each incidence and each flow velocity. An example of vibration spectra is given on Figure

7, which represents the spectra with α = 8° depending on the flow velocity.

α (°)	3 m.s^{-1}	4 m.s^{-1}	5 m.s^{-1}	6 m.s^{-1}
0	35 186	37 186.5	36 190	37 184.5
2	36.5 186.5	37.5 187	37 186.5	37 189.5
4	37.5 187	35.5 187.5	36.5 187	36 189
6	37 185	36.5 188.5	37 190	36.5 190.5
8	36.5 182	35.5 188.5	37 191	37 194

Table 3: First two modes frequencies (Hz) depending on the flow speed and the AoA

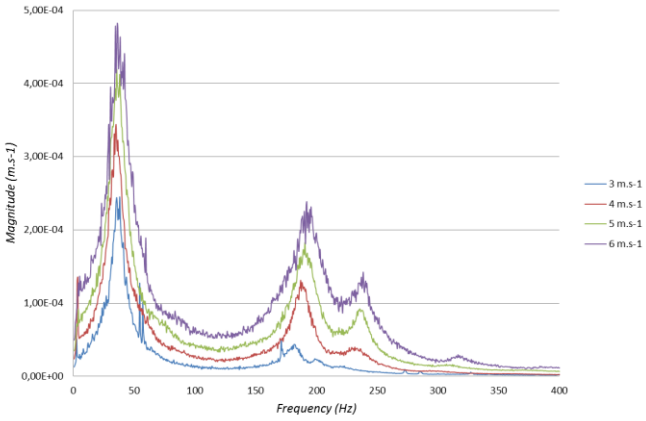

Figure 7: Spectra with α = 8°, U = 3 to 6 m.s^{-1} at atmospheric pressure (non cavitating flow)

The first mode's frequency is constant with the flow speed and the angle of attack, whereas the second and the third one's increase slowly with the flow speed (Figure 7). For the lowest incidences (0 to 4°) and flow velocities (3m.s^{-1}), a high peak appears near the twisting mode's frequency. It is a consequence of unsteadiness of a laminar separation bubble (LSB) inducing transition at low angle of attack on the rear part of the suction side (Ducoin et. al. (2012a)). These peaks disappear when the incidence or the velocity increases. It is explained by the sudden displacement of the LSB and transition towards the leading edge (Delafin et.al. (2014)).

3.2 Cavitating flow

To study the behavior of the flexible foil with cavitation, measurements have been carried out by decreasing the pressure. The cavitation number is defined by

$$\sigma = \frac{(P_0 - P_v)}{0.5\rho U^2}$$

where P_0 is the pressure at middle of the test section, P_v the vapor pressure at the water temperature, U the flow velocity and ρ the water density. The cavitation was controlled by decreasing or increasing the pressure P_0 at a fixed velocity.

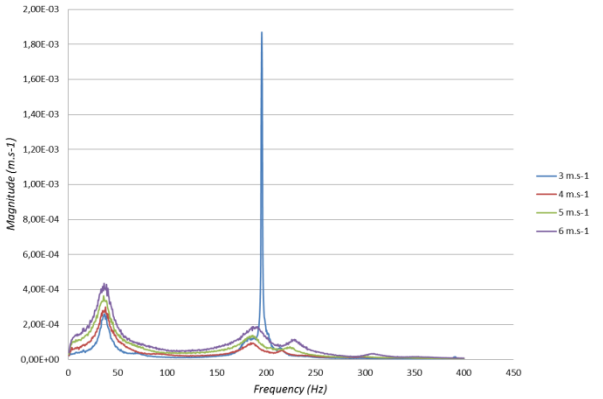

Figure 8: Spectra with α = 2°, U = 3 to 6 m.s^{-1} at atmospheric pressure (non cavitating flow)

Tests have been performed with a fixed flow velocity (U = 6 m.s^{-1}) and two angles of attack (α = 8, 10°). For α equal to 8°, eight measurements have been performed, that corresponds to cavitation numbers ranging between σ = 1.52 and σ = 5.68 (wetted flow). For α equal to 10°, six measurements have been carried out with σ decreasing from 2.51 to 1.52. The spectra are shown on Figure 9 and Figure 10.

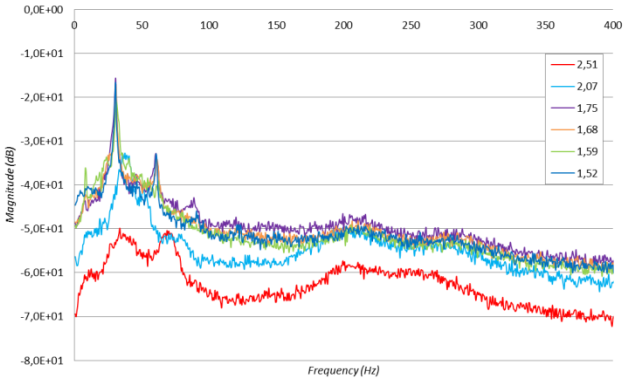

Figure 9: Response of a foil in cavitating flow, α = 10°, U = 6m.s^{-1}

As shown on Figure 10, the frequencies of the twisting and the third modes increase as σ decrease. On the contrary, the bending mode's frequency tends to decrease slightly as the cavitation develops. For the lowest cavitation numbers (σ lower than 1.41), a low frequency peak and its harmonics appear. For α = 8°, the first peak corresponds to the bending mode's frequency and is steady until σ = 1.6, then it falls to 8Hz. The same trend is visible on the curves with α = 10°, but the fall seems to occur later.

To study this phenomenon, films have been recorded to observe the flow and the cavitating flow. For α equal to 8° and p = 460 mbar (σ = 2.42), attached bubbles appear on

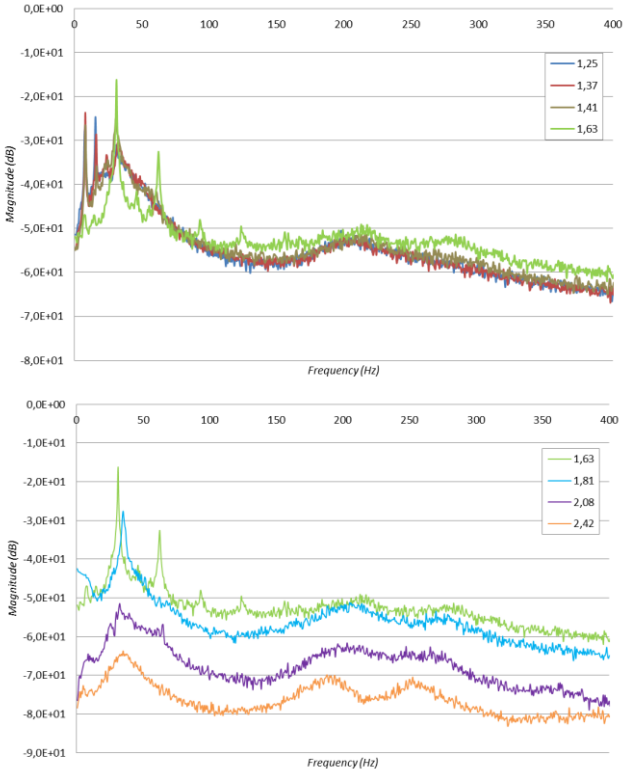

Figure 10: Vibration spectra in cavitating flow, α = 8°, U = 6m.s^{-1} (Spectra are displayed on two subfigures (a) and (b) depending on σ to improve visibility, the green curve (σ = 1.63) is represented on both figures).

the foil due to surface irregularities (Figure 11). As the pressure decrease, a bigger bubble appears and oscillate between 20 and 50% of the chord (σ = 2.08). The frequency of these oscillations is close to the bending mode's frequency of the foil, what implies a lock-in between both frequencies and a strong increase of the magnitude of the peak. A second peak corresponding to the harmonic of this frequency appears and develops with cavitation.

For σ = 1.81 and 1.63 (Figure 12), this oscillation becomes important. The cavity oscillates from 0 to 70% of the chord length before being carried away downstream. The frequency of the cavity oscillation, called f_o, can be computed thanks to the high speed camera records between two periods of the cavity evolution. The frequencies correspond to the higher peaks of the frequency responses, that could explain the decrease of the first peak's frequency from the bending mode frequency (around 37Hz) to 30Hz. Harmonics of this frequency are observed for σ = 1.63.

As the cavitation number becomes lower than σ = 1.41, a peak appears at f = 8Hz (Figure 13). Its harmonics are first relatively low but interact with the bending 30Hz-peak. As the pressure decreases again (σ = 1.37 and 1.25), this interaction disappears and the first harmonic becomes stronger. This low frequency peak corresponds to the oscillation frequency of the cavity: it oscillates from 0 to

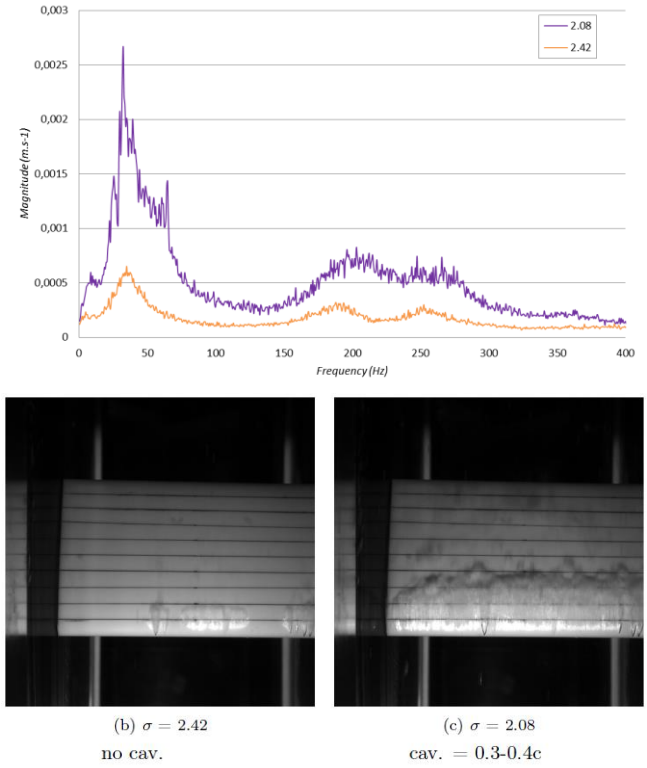

(b) $\sigma = 2.42$ no cav.

(c) $\sigma = 2.08$ cav. = 0.3-0.4c

Figure 11: Snapshots of cavitating flow and corresponding vibration spectra, α = 8°, U = 6m.s^{-1}

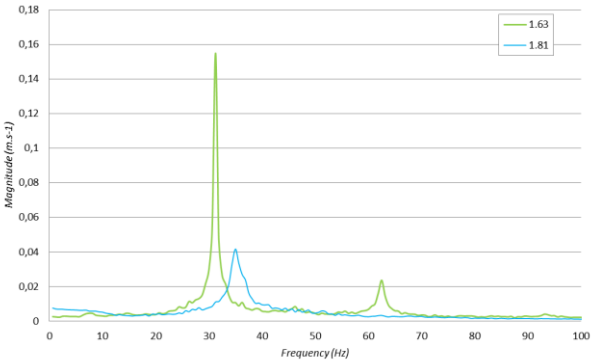

(b) $\sigma = 1.81$ cav. = 0.3-0.6c

(c) $\sigma = 1.63$ cav. = 0-0.7c

Figure 12: Snapshots of cavitating flow and corresponding vibration spectra, α = 8°, U = 6m.s^{-1}

100% of the chord length.

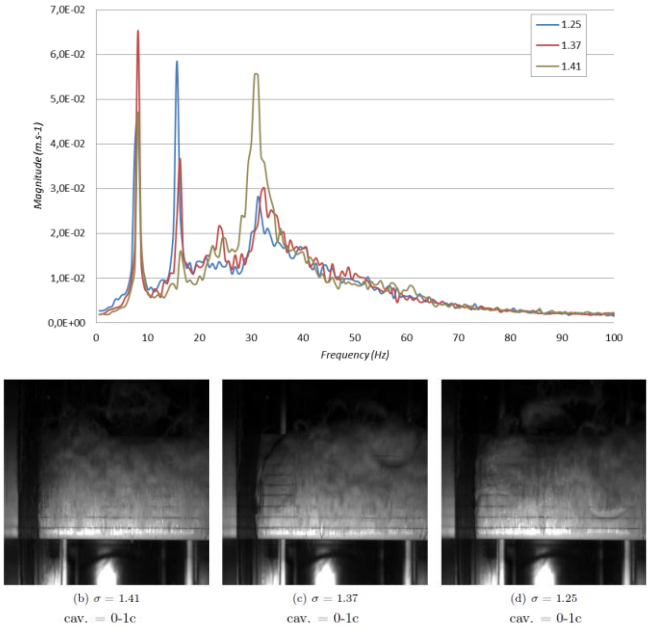

Figure 13: Snapshots of cavitating flow and corresponding vibration spectra, $\alpha = 8°$, $U = 6m.s^{-1}$

The Table 4 gathers the oscillation frequencies f_o and the main frequencies of the foil, called f_m, depending on the cavitation number.

σ	2.42	2.08	1.81	1.63	1.41	1.37	1.25
f_o	-		33	31.4	8.51	8.54	7.84
f_m	35	32.5	35	31	8	8	8

Table 4: Oscillation frequencies of the cavity sheet and main frequencies of the foil depending on the cavitation number

The same phenomenon appear with $\alpha = 10°$. For $\sigma = 2.51$ and $\sigma = 2.07$, a sheet cavitation oscillates between 20% and 40%, and between 0 and 50% respectively, but no frequency appears distinctly on the films. Then we can observe a growth of the cavity until the shedding with a measurable frequency value of approximately 30.3Hz for $\sigma = 1.75$ and 33Hz for $\sigma = 1.59$, very close to bending frequency.

4 STRAINS AND STRESSES' ANALYSIS

4.1 Static configuration

Concerning strains' measurements, the experiment was performed from -10° to 10° and with a step $\Delta\alpha = 0.5°$, at flow velocity $U = 5m.s^{-1}$. The values of ε_i are recorded during 10 seconds and the mean value computed. In order to study the strains resulted from the flow only, the values in still water are removed. Then, as the hydrofoil section is symmetrical, the strains are null for $\alpha = 0°$. This allows us to adjust precisely the value of the incidence α_0 during the experiments.

The results are shown on the Figure 14. It is observed that the hydrofoil behaves like a built-in beam: ε_1 and ε_2 increases with the angle of attack. The higher strain is ε_1, which corresponds to the span direction (blue line on the Figure 14). It is due to the hydrodynamic forces, particularly the lift. The strain ε_3 (green line) is opposed to the others because of the twist and the shearing stress.

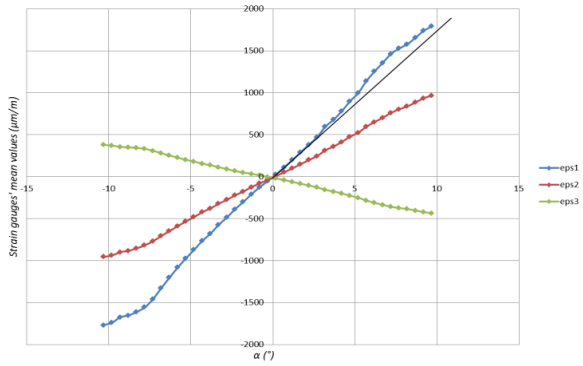

Figure 14: Strains (µm/m) depending on the AoA, $U = 5m.s^{-1}$

It is observed that the strains are linear up to 3° (see the straight line on Figure 14). Then they discard from the linear trend. This is particularly true for ε_1 that is highly related to the lift. This is a consequence of the lift forces that has been found to evolve in the same way as a result a boundary layer transition due to a LSB (Delafin, et al. (2014)). It was observed that triggering the boundary layer at the leading edge suppress the peculiar nonlinear behavior of lift.

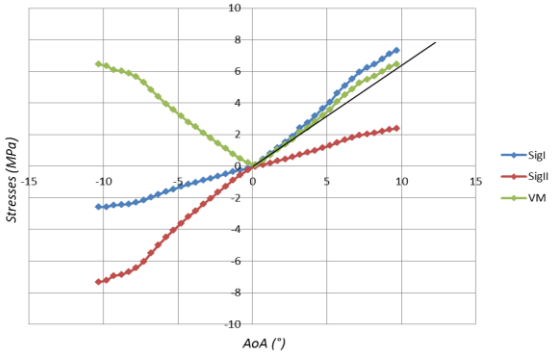

Figure 15: Principal stresses and Von Mises stresses (MPa) depending on the AoA, $U = 5m.s^{-1}$

Figure 15 shows the principal stresses (Equation (2)) and the Von Mises stresses (Equation (3)). As shown, an inversion of the principal stresses' curves appears passing through 0°. This is due to a change of the principal directions. The Von Mises stress is symmetrical and it is linear up to 4° (respectively -4° for negative angle of incidence). Beyond it discards from the linear evolution as a result of a similar evolution of the lift coefficient.

4.2 Cavitating flow

Measurements have been carried out with a decreasing number of cavitation in order to analyze the behavior of the strains and stresses in cavitating flows. It was observed that the mean values of the strains ε_i seem to decrease with σ, as it is illustrated by the Figure 16. In the same time, the fluctuations of the signal increase, as shown by the vertical bars, determined by the standard deviation. This is particularly true for ε_1. The same phenomenon is observed with the principal stresses and the Von Mises stresses as well (Figure 17).

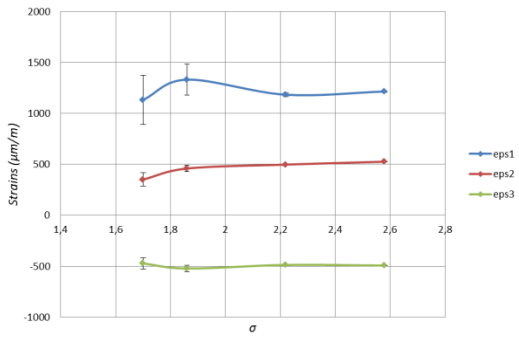

Figure 16: Mean ε_i depending on σ. Vertical bars are determined by the standard deviation.

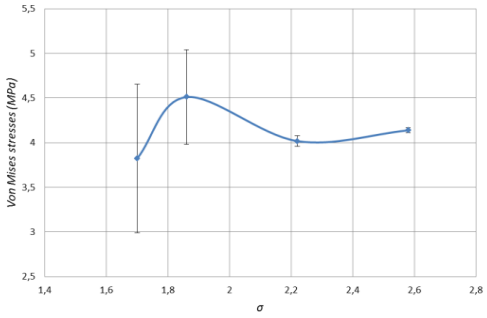

Figure 17: Mean values of Von Mises stresses depending on cavitation. Vertical bars are determined by standard deviation.

As the cavitation number decrease, the strain signals experience large fluctuations at a given frequency related to the oscillation of the cavity. The frequency, called f_c, decreases as the cavity increases. This is clearly shown on Figure 18, which represents the time series of the Von Mises stresses depending on the cavitation number.

The main frequencies are reported on Table 5 depending on the cavitation number. The frequencies of the strain gauges' signals are similar to the vibration's frequencies of the foil, which were observed earlier, considering the number of cavitation. It is particularly clear on the Von Mises stresses' signal with $\sigma = 1.70$ (Figure 18).

Pressure (mbar)	σ	f_c (Hz)
340	2.58	33.7
295	2.22	33
252	1.86	28
230	1.70	6.8

Table 5: Main frequencies of the strain gauges' signals

A fall of the main frequency appears then when σ decreases. However, the natural frequencies don't disappear and secondary oscillations with a 30 Hz-frequency are still observable on the curves.

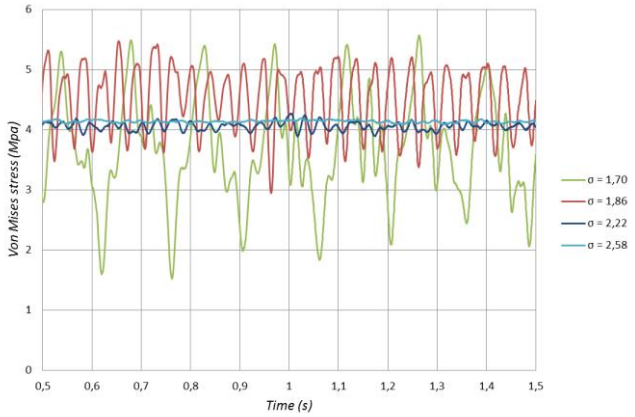

Figure 16: Time-history of Von Mises stresses for different cavitation number

5 CONCLUSIONS AND FUTURE WORK

An experimental procedure was developed to analyze the vibrations, the strains, and the stresses of a rectangular, cantilevered and flexible NACA 0015 made in POM, in sub-cavitating flow and in unsteady partial cavitation. The experiments were performed in the cavitation tunnel of the Naval Academy Research Institute. The hydrofoil was equipped with three identical strains gauges imbedded close to the root of the foil.

Vibrations measurements were carried out using two laser vibrometers in sub-cavitating and in cavitating flows. First the bending and twisting mode's frequencies were identified thanks to impulses on the foil's surface in the air and in still water. Then measurements at atmospheric pressure were performed for various flow velocities corresponding to Reynolds number ranging from 3. 10^5 to 6.10^5, and various angle of attack (AoA) from 0° to 8°. It is observed that the bending mode's frequency is nearly constant as the AoA or the flow velocity increases. On the other hand, the twisting mode's frequency increases with the flow velocity. A peculiar vibration phenomenon was observed at relatively low AoA. It induced a strong peak at a given frequency that can be related to a laminar separation bubble, which disappears as the AoA or the velocity increases. The measurements carried out by decreasing the pressure allowed us to notice that the bending mode's frequency changes depending on the oscillation frequency of the cavity, resulting from a lock-in phenomenon with the

cavity oscillation's frequency. Moreover, the twisting mode's frequency tends to increase with the cavity length that could be related to a decrease of the added mass effects.

In cavitating flow, the average value of the strains and stresses tend to decrease as the cavitation develops, whereas the fluctuations of the signal increase.

This work has to be followed with different enhancements. In particular, the force measurement on flexible foil should be improved. Moreover, tests will be performed with other foils made of more flexible materials. It will help to continue the study of the fluid-structure interactions between the flow and the foil in different conditions.

ACKNOWLEDGMENTS

The authors wish to acknowledge the Office of Naval Research for the support under the grant number N62909-12-1-7076, as well as the technical staff of the Naval Academy Research Institute, Alain Boulch is gratefully acknowledged.

REFERENCES

Akcabay, D. T., Chae, E. J., Young, Y. L., Ducoin, A., and Astolfi, J. A. (2014), "Cavity induced vibration of flexible hydrofoils", Journal of Fluids and Structures, 49, 463-484.

Akcabay, D. T., Young, Y. L. (2014), "Influence of cavitation on the hydroelastic stability of hydrofoils", Journal of Fluids and Structures, 49, 170-185.

Benaouicha, M., Astolfi, J. A., Ducoin, A., Frikha, S. and Coutier-Delgosha, O. (2010). "A Numerical Study of Cavitation Induced Vibration". Proc. of Pressure Vessels and Piping Conference, Washington, USA.

Benaouicha, M. and Astolfi, J. A. (2012), "Analysis of added mass in cavitating flow" Journal of fluids and structures, 31, 30-48.

Brennen, C. E. (1995), "Cavitation and Bubble Dynamics." Oxford University Press.

Coutier-Delgosha, O., Stutz, B., Vabre, A. and Legoupil, S. (2007), "Analysis of cavitating flow structure by experimental and numerical investigations" Journal of Fluid Mechanics, 578, 171–222

Delafin, P. L., Deniset, F., and Astolfi, J. A. (2014), "Effects of the laminar separation bubble induced transition on the hydrodynamic performance of a hydrofoil" European Journal of Mechanics/B, 46, 190-200.

Ducoin, A., Deniset, F., Astolfi, J. A. and Sigrist, J.-F. (2009). "Numerical and Experimental Investigation of Hydrodynamic Characteristics of Deformable Hydrofoils", Journal of Ship Research, 53, 214-226

Ducoin, A., Astolfi, J. A., and Gobert, M. L. (2012a). "An experimental study of boundary layer transition induced vibrations on a hydrofoil" Journal of Fluids and Structures, 32, 37-51.

Ducoin, A., Astolfi, J. A., and Sigrist, J.-F. (2012b), "An experimental analysis of fluid structure interaction on a flexible hydrofoil in various flow regimes including cavitating flow", European Journal of Mechanics/B, 36, 63-74.

Franc, J. P., (2006), "Physics and control of cavitation", Design and analysis of high speed pumps. 2.1-2.36.

Gaugain, F., Deniset, F., Astolfi, J. A. and Sigrist, J. F. (2012), "Numerical and Experimental Study of Hydroelastic Behaviour of a Hydrofoil" Proc. of 10th International Conference on Flow-Induced Vibrations, Dublin, 67-74

Leroux, J. B., Coutier-Delgosha, O. and Astolfi, J. A. (2005), "A joint experimental and numerical study of mechanisms associated to instability of partial cavitation on two-dimensional hydrofoil" Physics of Fluids, 5, 052101

Lin, H. J., Lin, J. J. and Chuang, T. J. (2005). "Strength Evaluation of a Composite Marine Propeller Blade". Journal of Reinforced Plastics and Composites, 24, 1791-1807.

Motley, M. R., and Young, Y. L. (2011), "Performance-based design and analysis of flexible composite propulsors" Journal of Fluids and Structures, 27, 1310-1325.

Mulcahy, N. L., Prusty, B. G., and Gardiner, C. P. (2010), "Flexible Composite Hydrofoils and Propeller Blades" Proc. of International Maritime Conference 2010: Maritime Industry - Challenges, Opportunities and Imperatives, Sydney, Australia, 438-448.

Reese, M. C. (2010), "Vibration and damping of hydrofoil in uniform flow", Thesis, Pennsylvania State University

Søntvedt, T. (1974), "Propeller blade stresses, application of finite element methods", Computers & Structures, 4, 193-204

Young, Y. L. (2007) "Hydroelastic behavior of flexible composite propellers in wake inflow" Proc. of 16th International Conference on composite materials, Kyoto Japan.

Young, Y. L. (2008) "Fluid–structure interaction analysis of flexible composite marine propellers" Journal of Fluids and Structures, 24, 799-818.

Young, Y. L., Motley, M. R. and Yeung, R. W. (2009) "Hydroelastic Response of Wind or Tidal Turbines" Proc. of 28th International Conference on Ocean, Offshore and Arctic Engineering, Honolulu, USA, 1101-110

DISCUSSION

Question from Mario Felli

Wavelet is a very powerful technique for the analysis of such problems. Is the use of wavelets in your plans for future works?

Author's closure

Yes, we plan to use several methods of decomposition and using wavelets is one of them. Time frequency analysis based on Empirical Modal Decomposition and instantaneous frequency analysis for instance is a method that should provide interesting results, especially for large cavity fluctuations.

Questions from Yin Lu Young

Experimental studies conducted by Ms. Lelong for POM NACA0015 and by Dr. Ducoin for POM NACA66 both shown that the higher mode natural frequencies increase with decreasing sigma due to decreasing of added mass.

Combined experimental and numerical studies of the influence of varying added mass and damping due to unsteady cavitation have been presented in the following reference: Akcabay, D. T., Young, Y. L., Lelong, A., Astolfi, J. A. (2014), "Cavity Induced Vibrations of Flexible Hydrofoils and their Susceptibility to Lock-in and Parametric Excitations", 30th Symposium on Naval Hydrodynamics

Author's closure

I agree with the comment definitively. A point that needs to be closely studied concerns the influence of the cavity oscillation on the modal frequencies. Indeed, in that case of cavity oscillation, the added mass could oscillate as well as lead to a Fluid Structure System with time variation of the mass that is quite different of a system with a constant mass. The question of instantaneous frequency should be addresses as well. This point was primarily addressed theoretically in a paper by Benaouicha and Astolfi (2012). They showed that the added mass matrix might not be symmetric in partial cavitating flow.

Question from Antoine Ducoin

You show that decreasing sigma leads to lock-in of cavity shedding frequency with the natural frequency of the structure. The higher sigma show however only one peak, that suggests that you have also lock-in condition with a lower sigma.

Author's closure

This point needs to be studied. However, the question of the deflection of relative small cavity oscillation on the vibration spectrum at higher cavitation number (with maximum cavity length smaller than about half the chord length) should be addressed as well.